Acta Crystallographica Section A
Foundations of Crystallography
ISSN 0108-7673

Received 25 February 2004
Accepted 21 July 2004

The experimental electron density in polymorphs A and B of the anti-ulcer drug famotidine

Jacob Overgaard* and David E. Hibbs

School of Chemistry, University of Sydney, Australia. Correspondence e-mail: jacobo@chem.usyd.edu.au

Accurate structure factors have been measured for the two known conformational polymorphs (A and B) of famotidine up to a maximum resolution of $\sin(\theta)/\lambda = 1.2$ Å^{-1} at 100 K using a conventional X-ray source and a CCD-based diffractometer. The experimental electron-density distribution was modelled using a multipole model and the interatomic interactions were analysed following the atoms-in-molecules theory. Excellent equivalence between most electronic and electrostatic properties in the polymorphs exists and no significant differences were found to exist across polymorphs either in the interatomic interactions (*via* the topological analysis) or in the atomic charges from integration of the atomic basins. Additional derived properties, such as the molecular dipole moment, similarly did not distinguish between the polymorphs. Only the molecular electrostatic potential mapped on top of the molecular surface, *i.e.* the isodensity contoured at 0.00675 e Å^{-3}, was able to uncover the differences between A and B. In both conformations, the sizes of the electronegative and electropositive areas match. However, the average electrostatic potential in the electronegative area of A is -40 kJ mol^{-1}, while the corresponding value in B is -55 kJ mol^{-1}. Together with the physical shape and dimensions of A and B, this leads to a conclusion that the polymorphs are mutually exclusive at the same receptor binding site.

1. Introduction

Famotidine is the lesser known generic name for the tremendously successful anti-ulcer drug known under the trade name Pepcid. Famotidine belongs to a diverse class of histamine H_2-receptor antagonists whose properties were first recognized by Black and co-workers at Smith, Kline and French Laboratories by their discovery of the antagonist activity of cimetidine (Brimblecombe *et al.*, 1975). A number of structural features of this class of antagonists are required for any antagonist activity to be exhibited, such as the five-membered heteroatomic aromatic ring and the S atom in the alkane chain.

However, only a very limited proportion of the literature on anti-histamine agents has been devoted to the problematic issue of polymorphism in the crystal structures of these molecules. In the case of famotidine, the two known polymorphs were prepared in 1986 by the Hungarian pharmaceutical company, Gedeon Richter (Gedeon Richter Ltd, 1986). Recent work, partly by the same research group, leads to the conclusion that, of the two significantly different molecular forms, polymorph A is the thermodynamically favoured form, while polymorph B is the kinetically favoured form of famotidine (Ferenczy *et al.*, 2000). However, the group's theoretical results also indicate that the two forms are almost equally stable; hence, the molecular structure of famotidine *in vitro* is not easily extracted from solid-state experiments and more work on these structures is certainly required for further understanding.

From a charge-density point of view, the study of polymorphic compounds remains a challenge and is potentially highly rewarding. Fewer than a handful of papers have been published dealing with the experimentally derived electron-density distribution in polymorphic structures (Gopalan *et al.*, 2000; Kulkarni *et al.*, 1998, 2000; Whitten *et al.*, 2004). However, it is common to all of the three first papers that the molecular structures reported are almost completely rigid and the major differences between the polymorphs are different packing schemes. In this contribution, we report the experimental electron-density distribution in the two markedly different known molecular conformations of famotidine.

2. Experimental

High-quality single crystals of both polymorphs were kindly donated by Dr B. Hegedus of Chemical Works at Gedeon Richter Ltd.

2.1. X-ray diffraction data collection and reduction

The X-ray single-crystal diffraction experiments were carried out at the University of Sydney using a Bruker

Table 1
Experimental details.

	(IA)	(IB)
Formula	$C_8H_{15}N_7O_2S_3$	$C_8H_{15}N_7O_2S_3$
FW (g mol^{-1})	337.45	337.45
Crystal system	Monoclinic	Monoclinic
Space group	$P2_1/c$	$P2_1/n$
Z	4	4
a (Å)	11.9115 (3)	16.980 (2)
b (Å)	7.1876 (2)	5.285 (1)
c (Å)	16.6236 (4)	17.639 (2)
α (°)	90	90
β (°)	100.045 (1)	116.416 (1)
γ (°)	90	90
V (Å^3)	1401.4 (1)	1418.0 (4)
No. of reflections for cell refinement	16250	8948
θ_{min}–θ_{max}	2.3–59.3	2.2–29.5
F(000)	504	504
T (K)	100	100
ρ (g cm^{-3})	1.595	1.561
μ(Mo $K\alpha$) (mm^{-1})	0.54	0.53
T_{max}, T_{min}	0.887, 0.787	N/A
d_{min} (Å)	0.41	0.41
Data reduction		
N_{meas}, N_{uniq}	68907, 20197	70467, 21282
Redundancy	3.4	3.3
Completeness	96.6	97.7
No. of discarded reflections	5065	2160
h, k, l ranges	−28→28, 0→17, 0→39	−41→37, 0→12, 0→43
R_{int}	0.020	0.025
Refinement		
N_{obs}, N_{var} (σ cut-off)	16610, 459 (2)	17385, 459 (2)
$R_w(F)$, $R_w(F^2) > 2\sigma(F)$	0.021, 0.039	0.021, 0.039
$R(F)$, $R(F^2)$, all data	0.040, 0.025	0.040, 0.029
Goodness of fit	1.70	1.62

SMART1000 CCD-based diffractometer with an X-ray wavelength of 0.7107 Å (Mo $K\alpha$) and an experimental temperature of 100 K. The crystals were mounted on the tip of a thin glass fibre with a minimum amount of Paratone N oil and inserted in the cold N_2 stream from an Oxford Cryosystems device. Each experiment was completed in six to seven days, collecting approximately 10000 reflections per day. In this way, nearly all (∼97%) independent reflections below a resolution level of 1.20 Å^{-1} were measured with average remeasurement ratios of 3.3.

The collected intensities were integrated using *SAINT+* (Bruker, 1999). Subsequently, *SORTAV* (Blessing, 1997) was used to perform a face-indexed Gaussian absorption correction (only for polymorph A) followed by intensity scaling and averaging. In this process, 3 and 7% of the measured reflections were discarded for famotidine A and B, respectively, mainly due to the reflections having a forbidden symmetry according to the space group. Table 1 presents the experimental details for famotidine.[1]

[1] Supplementary data for this paper, including CIFs, structure factors and density maps, are available from the IUCr electronic archives (Reference: XC5012). Services for accessing these data are described at the back of the journal.

2.2. Structure and multipole refinement

Both molecular structures were solved using direct methods with the program *SHELXS* (Sheldrick, 1997) and these models were imported into *SHELXL-97* (Sheldrick, 1997) for refinement within the restraints of the independent-atom-model (IAM). The positions and anisotropic thermal parameters were refined for all non-H atoms, while the H atoms – after being located in a difference Fourier synthesis – were refined to move at fixed distances from their parent atom with independent isotropic thermal motion. The final structural models for famotidine A and B (see Fig. 1) were exported to the program *XD* (Koritsanszky *et al.*, 2003) for multipole refinement, in which the progress towards – as well as the complexity of – the final model was identical for famotidine A and B. This is a central point in the strategy since the aim of this study is to compare the properties of the two electron-density distributions without introducing any unwarranted errors.

The program *XD* uses a least-squares procedure to refine a rigid pseudoatom model in the form of the Hansen–Coppens multipole formalism (Hansen & Coppens, 1978):

$$\rho_{atomic}(r) = P_{core}\rho_{core}(r) + P_{val}\rho_{val}(r)\kappa^3 + \sum_{l=0}^{l_{max}} R_l(\kappa' r)\kappa'^3 \sum_{m=0}^{l} P_{lm\pm} d_{lm\pm}(\theta, \varphi). \quad (1)$$

In these multipole refinements, up to and including hexadecapoles were refined for all S atoms, while the maximum level of multipoles was octupoles for all other non-H atoms. For the H atoms, only monopoles and bond-directed dipoles were used. A limited number of constraints were introduced in the refinement procedure to ensure that as much as possible

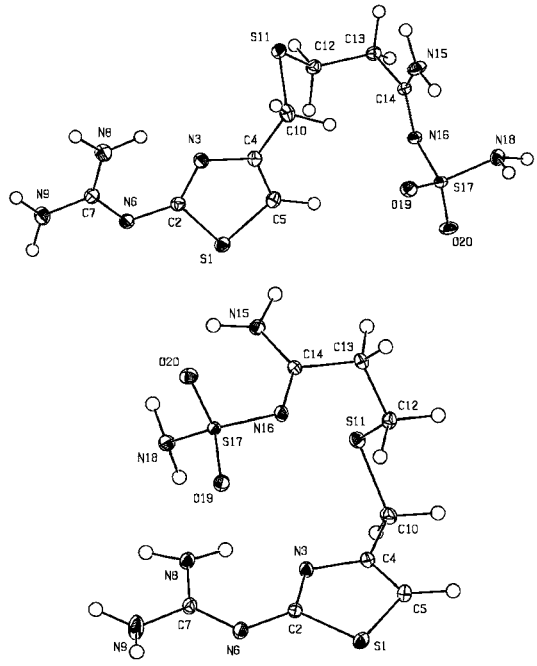

Figure 1
Thermal ellipsoid plot of the two polymorphs A and B of famotidine. The ellipsoids are outlined at the 50% probability level.

Table 2
Selected bond distances (Å) and angles (°) for the bonds not involving H in famotidine A and B.

Bond	(IA)	(IB)	Angle	(IA)	(IB)
S(1)—C(2)	1.7594 (3)	1.7542 (3)	C(2)—S(1)—C(5)	89.67 (1)	89.62 (1)
S(1)—C(5)	1.7301 (3)	1.7278 (4)	C(10)—S(11)—C(12)	101.72 (1)	99.56 (2)
S(11)—C(10)	1.8320 (4)	1.8205 (3)	O(19)—S(17)—O(20)	117.08 (2)	116.82 (2)
S(11)—C(12)	1.8131 (3)	1.8129 (3)	O(19)—S(17)—N(16)	111.65 (2)	104.25 (2)
S(17)—O(19)	1.4473 (3)	1.4387 (3)	O(19)—S(17)—N(18)	105.51 (2)	106.74 (2)
S(17)—O(20)	1.4397 (3)	1.4501 (3)	O(20)—S(17)—N(16)	104.70 (2)	111.39 (2)
S(17)—N(16)	1.6136 (2)	1.6090 (3)	O(20)—S(17)—N(18)	111.38 (2)	105.02 (2)
S(17)—N(18)	1.6311 (2)	1.6118 (3)	N(16)—S(17)—N(18)	106.11 (1)	112.75 (2)
N(3)—C(2)	1.3234 (4)	1.3177 (4)	C(2)—N(3)—C(4)	111.34 (2)	111.75 (3)
N(3)—C(4)	1.3858 (4)	1.3764 (4)	C(2)—N(6)—C(7)	120.42 (3)	119.31 (3)
N(6)—C(2)	1.3548 (4)	1.3622 (4)	S(17)—N(16)—C(14)	120.81 (2)	124.38 (2)
N(6)—C(7)	1.3390 (3)	1.3329 (4)	S(1)—C(2)—N(3)	113.26 (2)	113.10 (2)
N(8)—C(7)	1.3392 (4)	1.3425 (4)	S(1)—C(2)—N(6)	116.59 (2)	118.04 (2)
N(9)—C(7)	1.3425 (4)	1.3457 (4)	N(3)—C(2)—N(6)	130.15 (3)	128.85 (3)
N(15)—C(14)	1.3223 (4)	1.3267 (4)	N(3)—C(4)—C(5)	115.72 (3)	115.62 (3)
N(16)—C(14)	1.3266 (3)	1.3179 (4)	N(3)—C(4)—C(10)	118.38 (2)	119.11 (3)
C(4)—C(5)	1.3654 (4)	1.3627 (4)	C(5)—C(4)—C(10)	125.90 (3)	125.26 (3)
C(4)—C(10)	1.4919 (4)	1.4938 (4)	S(1)—C(5)—C(4)	109.97 (2)	109.88 (2)
C(12)—C(13)	1.5404 (4)	1.5272 (4)	N(6)—C(7)—N(8)	124.65 (3)	124.93 (3)
C(13)—C(14)	1.5050 (4)	1.5142 (4)	N(6)—C(7)—N(9)	117.51 (3)	118.26 (3)
			N(8)—C(7)—N(9)	117.83 (3)	116.81 (3)
			S(11)—C(10)—C(4)	113.31 (2)	114.03 (2)
			S(11)—C(12)—C(13)	114.66 (2)	109.96 (2)
			C(12)—C(13)—C(14)	111.65 (2)	112.53 (2)
			N(15)—C(14)—N(16)	127.23 (3)	128.26 (3)
			N(15)—C(14)—C(13)	117.17 (2)	116.77 (3)
			N(16)—C(14)—C(13)	115.56 (2)	114.97 (2)

the final refined models represent the global energy minima (El Haouzi *et al.*, 1996): Firstly, the H-atom positions were fixed such that their bond distances corresponded to the generally accepted bond distances derived from neutron data (Allen *et al.*, 1987). Secondly, the multipoles for all H atoms bonded to N atoms were considered identical, as were the multipoles for H atoms bonded to C atoms. As a final constraint, the thiazole sulfur [S(1)] and the thioether sulfur [S(11)] atoms were both assigned C_{2v} symmetry, while C_s symmetry was imposed upon three N atoms and five C atoms.

The core and spherical valence densities were constructed from energy-optimized Hartree–Fock wavefunctions (Clementi & Roetti, 1974) while the radial function in the valence deformation density [third term in (1)] is a Slater-type function of the type $R_l(\kappa' r) = N_l r^{n(l)} \exp(-\kappa' \xi r)$. Recently, it has been suggested that the optimum n_l values for S atoms are 6, 6, 7, 7 for l = 1, 2, 3, 4 with a fixed ξ of 3.851 a.u. (Hibbs *et al.*, 2003) and these values were adopted in this study. For O, N and C atoms, n_l values of 2, 2, 3 were used for l = 1, 2, 3 and default values of ξ were used (4.47, 3.84, 3.18 a.u. for O, N and C atoms, respectively).

An important feature of the multipole model is the possibility to adjust the radial dependency for each atom type by including the expansion/contraction controlling κ parameters in the refinement, and possibly also the κ' parameters, to change the radial dependency of the valence deformation density. However, the refinement of the κ parameters (especially κ') is notoriously difficult and they are often only slowly converging; thus, these parameters are rarely refined freely. In the present study, the κ' parameters were refined in separate cycles together only with the scale factor, and convergence was achieved in an iterative process. Each refinement cycle was considered fully converged at the point at which the maximum shift/s.u. was less than 10^{-3}. To further assess the success of the refinement, Hirshfeld's rigid-bond test was applied after each step (Hirshfeld, 1976). With average values of the difference of mean square thermal displacement amplitudes of 3.5×10^{-4} and 2.6×10^{-4} Å^2 for A and B, respectively, and maximum values of 10×10^{-4} Å^2 for three of the S—C bonds, it can safely be assumed that the thermal motion is successfully deconvoluted from the electronic deformation due to bonding effects and hybridization.

3. Results and discussion

3.1. Structural details

Table 2 gives the intramolecular bond distances and angles for famotidine A and B, arranged side-by-side to enhance the ease of comparison. Firstly, it is noticed that the s.u.'s on the bond lengths are on the order of a few ten thousandths of 1 Å. A comparison of the values immediately reveals that the bond distances in A are almost consistently longer than for B. On average, this difference amounts to 0.003 Å or ~8σ. However, for a few bonds [of which the S(17)—O(20), N(6)—C(2) and C(13)—C(14) bonds are the most pronounced], the trend is reversed and the bond length in B is significantly longer and for this reason the difference cannot be attributed to an error in the unit-cell dimensions, which would reflect directly in the bond distances. On the other hand, no clear explanation for the discrepancies is apparent.

It is interesting to take a closer look at the geometries of the four different NH_2 groups, as it turns out that there are significant differences among them. Both structures exhibit entirely pyramidal NH_2 groups at N(18), and fully planar NH_2 groups at N(15). However, while the two NH_2 entities in the guanidine group are very nearly planar in A, famotidine B shows two NH_2 groups that are significantly pyramidalized [in A, the torsion angle N(6)—C(7)—N(9)—H(9*B*) is 2.5° and for N(6)—C(7)—N(8)—H(8*A*) it is 2.3°, while the corresponding angles in B are 17.6 and 11.9°, respectively]. A consequence of pyramidalization is the drawing nearer of the hydrogen pairs as quantified by a H(9*A*)—N(9)—H(9*B*) angle of 121.1 and 114.8° in A and B, respectively. It should be noted that these observations are made without the availability of neutron data.

Finally, the geometries in the tetrahedral SO_2N_2 sulfamoyl groups deserve a few comments, which will be elaborated upon in a later section. It is observed that the angular distribution is non-identical in A and B. Looking at the six central

Table 3
Results of the topological analyses of A and B, with first line showing the results for A and second line the results for B.

The units are: $[\rho_{b.c.p.}]$ e Å^{-3}, $[\nabla^2\rho_{b.c.p.}]$ e Å^{-5}.

Bond	$\rho_{b.c.p.}$	$\nabla^2\rho_{b.c.p.}$	ε	$d_{1\text{-b.c.p.}}$	$d_{2\text{-b.c.p.}}$	λ_1	λ_2	λ_3
S(1)—C(2)	1.36 (2)	−4.9 (1)	0.30	0.936	0.824	−8.76	−6.76	10.61
	1.34 (3)	−4.2 (1)	0.34	0.920	0.835	−8.78	−6.57	11.18
S(1)—C(5)	1.39 (2)	−4.2 (1)	0.23	0.919	0.812	−8.50	−6.91	11.20
	1.38 (3)	−4.1 (1)	0.30	0.909	0.820	−8.77	−6.75	11.40
S(11)—C(10)	1.13 (2)	−1.8 (1)	0.00	0.974	0.858	−6.10	−6.08	10.38
	1.16 (2)	−2.4 (1)	0.13	0.968	0.853	−6.87	−6.10	10.55
S(11)—C(12)	1.17 (2)	−2.2 (1)	0.11	0.962	0.851	−6.75	−6.09	10.60
	1.16 (2)	−2.6 (1)	0.17	0.968	0.845	−7.05	−6.03	10.48
S(17)—O(19)	2.37 (3)	0.8 (1)	0.02	0.599	0.848	−14.13	−13.85	28.78
	2.39 (3)	3.0 (1)	0.08	0.600	0.839	−15.16	−14.03	32.28
S(17)—O(20)	2.40 (3)	1.0 (1)	0.10	0.597	0.843	−14.80	−13.41	29.23
	2.33 (3)	1.6 (1)	0.16	0.606	0.845	−15.18	−13.03	29.81
S(17)—N(16)	1.82 (3)	−12.8 (1)	0.13	0.760	0.854	−11.97	−10.58	9.72
	1.90 (3)	−12.7 (1)	0.09	0.753	0.859	−11.92	−10.97	10.22
S(17)—N(18)	1.88 (3)	−13.6 (1)	0.14	0.791	0.840	−12.16	−10.69	9.26
	1.80 (3)	−11.7 (1)	0.17	0.727	0.885	−12.54	−10.67	11.54
N(3)—C(2)	2.64 (2)	−27.5 (1)	0.15	0.760	0.562	−21.74	−18.96	13.21
	2.65 (2)	−26.1 (1)	0.15	0.740	0.578	−22.13	−19.22	15.25
N(3)—C(4)	2.35 (2)	−18.4 (1)	0.08	0.759	0.627	−18.31	−16.96	16.92
	2.23 (2)	−17.6 (1)	0.06	0.779	0.598	−17.04	−16.10	15.50
N(6)—C(2)	2.52 (2)	−22.9 (1)	0.15	0.745	0.610	−21.07	−18.31	16.50
	2.43 (2)	−21.1 (1)	0.16	0.751	0.611	−20.3	−17.52	16.77
N(6)—C(7)	2.55 (2)	−26.6 (1)	0.19	0.762	0.577	−21.86	−18.33	13.61
	2.57 (2)	−25.5 (1)	0.12	0.737	0.596	−21.73	−19.40	15.65
N(8)—C(7)	2.57 (2)	−33.4 (1)	0.14	0.807	0.533	−22.94	−20.03	9.57
	2.55 (2)	−27.9 (1)	0.18	0.768	0.575	−22.55	−19.14	13.75
N(9)—C(7)	2.62 (2)	−29.8 (1)	0.25	0.772	0.570	−23.68	−18.90	12.82
	2.46 (2)	−28.9 (1)	0.24	0.808	0.538	−22.09	−17.78	10.98
N(15)—C(14)	2.55 (2)	−29.8 (1)	0.28	0.791	0.531	−22.67	−17.69	10.52
	2.52 (2)	−27.0 (1)	0.17	0.711	0.556	−21.43	−18.38	12.80
N(16)—C(14)	2.56 (2)	−25.1 (1)	0.19	0.740	0.587	−21.58	−18.19	14.66
	2.63 (2)	−25.7 (1)	0.17	0.741	0.578	−22.26	−19.00	15.60
C(4)—C(5)	2.31 (2)	−20.81 (4)	0.26	0.676	0.690	−17.80	−14.14	11.13
	2.28 (2)	−20.91 (5)	0.28	0.680	0.683	−18.13	−14.16	11.38
C(4)—C(10)	1.82 (1)	−13.69 (3)	0.13	0.747	0.745	−13.41	−11.87	11.59
	1.81 (2)	−12.77 (4)	0.11	0.758	0.736	−13.15	−11.89	12.27
C(12)—C(13)	1.65 (1)	−10.32 (3)	0.05	0.759	0.782	−11.23	−10.70	11.61
	1.64 (2)	−9.13 (3)	0.04	0.762	0.765	−10.87	−10.45	12.19
C(13)—C(14)	1.80 (1)	−13.71 (3)	0.12	0.707	0.798	−13.12	−11.69	11.09
	1.76 (2)	−11.64 (4)	0.09	0.719	0.795	−12.40	−11.34	12.10

angles at the S atom in this region, the values can be grouped in three categories – one high (~117°), two medium (~111°) and three low (~105°). It is common to A and B that the O—S—O angle is 117°, but the distribution of the medium and low values is different, and probably can be credited to differences in intermolecular N—H···O hydrogen bonding.

3.2. Analysis of the electron-density distribution

3.2.1. The sulfur atoms. As sulfur is positioned in the third row of the Periodic Table, it has available *d* orbitals, and a description of the charge distribution in the vicinity of an S atom is significantly more difficult to obtain than for the elements immediately above it in the Periodic Table, a tendency that is emphasized by the low number of experimental electron-density distribution studies of sulfur-containing compounds (Figgis *et al.*, 1993; McCormack *et al.*, 1996; Espinosa *et al.*, 1997; Scherer *et al.*, 2000; Pillet *et al.*, 2001; Hambley *et al.*, 2002; Leusser *et al.*, 2002, 2004). It is therefore reasonable first to examine the charge distribution in these regions to judge the reliability of the results extracted from the study.

In the famotidine molecule, three different S atoms are present, the thiazole S(1), the thioether S(11) and the sulfamoyl S(17) atoms. They possess the nominal oxidation numbers of −II for S(1) and S(11) and +VI for S(17). The supporting information contains the nearly featureless residual density maps that have been generated using the entire set of observed structure factors to a resolution of 1.20 Å^{-1}, as well as the static deformation density maps in a selection of planes.[2] However, to remove the inherent dependency on the use of a reference density distribution, which by definition exists in a static deformation density map, and instead provide an unbiased representation of the electron density, Fig. 2 shows the three-dimensional Laplacian distributions in regions near the atoms S(1) and S(17) for famotidine A. The situation is completely similar in famotidine B. The two lone

[2] See deposition footnote.

pairs that are expected for an sp^3-hybridized S(1) atom are clearly seen here [identical to the situation for S(11)], as are the shared interactions with its two neighboring C atoms. Fig. 2(*b*) shows the four shared interactions of S(17).

3.2.2. Topological analysis. In recent years, it has certainly become the standard in charge-density studies to attempt a quantitative description of the bonding by performing a topological analysis of the density following the theory of atoms in molecules advanced by Bader and his group (Bader, 1990). This methodology is particularly important in the studies of polymorphs where the differences in density distributions are likely to be small and a precise and quantitative tool is required to discover potential correlations between the physical properties and the molecular density distributions.

Table 3 outlines the most relevant topological parameters at the bond critical points (b.c.p.) between non-H atoms. The sign of $\nabla^2\rho_{\rm b.c.p.}$ is commonly used to categorize a particular bond as either ionic (positive $\nabla^2\rho_{\rm b.c.p.}$) or covalent (negative $\nabla^2\rho_{\rm b.c.p.}$); however, recently it has been shown that this view is probably too simplistic, both for covalent bonds and in metal–ligand interactions (Macchi *et al.*, 1998; Hibbs *et al.*, 2003), and a closer examination of the Laplacian along the entire bond path is required, as well as a comparison of the three individual curvatures, λ_{1-3}.

While studying Table 3, it quickly becomes apparent that the two molecules exhibit very similar topological bond characteristics, an indication of the extent to which reproducibility can be expected by this method. However, a few discrepancies are also revealed, of which the largest occurs in the N(8)—C(7) bond of the guanidine moiety in which $\nabla^2\rho_{\rm b.c.p.}$ differs by 5.5 e Å^{-5} between A and B, while the other N—C bond in this functional group, N(9)—C(7), shows a difference in $\rho_{\rm b.c.p.}$ of 0.16 e Å^{-3} between A and B. These differences may correlate with the different structural arrangements in the two guanidine amino groups. In famotidine B, the groups are less planar and more pyramidalized than in A, and this causes the N—C interactions to differ. If a common, but somewhat simplistic, approach is followed which assumes the magnitude of $\rho_{\rm b.c.p.}$ to be proportional to bond strength, the more planar amine group (famotidine A) exhibits the stronger N—C bond.

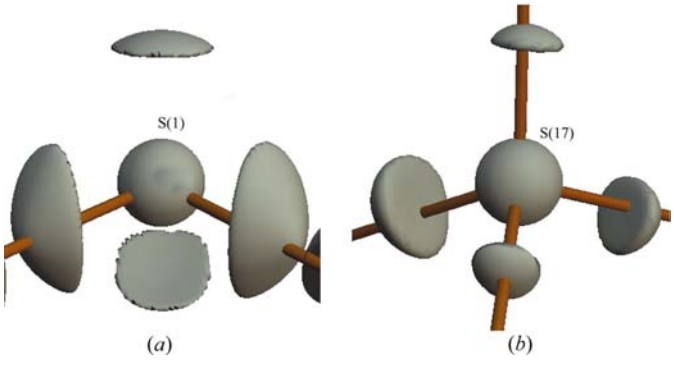

Figure 2
Three-dimensional Laplacian of the electron density in famotidine A showing (*a*) the thiazole S(1) and (*b*) the sulfamoyl S(17). The isosurfaces are outlined at −5 e Å^{-5}.

Table 4
Topological (Bader) atomic charges in A and B from integration of the atomic basins, in atomic units.

Atom	$q_{\rm A}(\Omega)$†	$q_{\rm B}(\Omega)$	Atom	$q_{\rm A}(\Omega)$	$q_{\rm B}(\Omega)$
S(1)	+0.22	+0.28	H(10*A*)	+0.19	+0.21
S(11)	+0.09	+0.15	H(10*B*)	+0.23	+0.21
S(17)	+2.69	+2.79	H(12*A*)	+0.19	+0.22
O(19)	−1.26	−1.26	H(12*B*)	+0.21	+0.20
O(20)	−1.31	−1.27	H(13*A*)	+0.19	+0.22
N(3)	−0.93	−1.02	H(13*B*)	+0.19	+0.21
N(6)	−1.04	−0.98	H(5)	+0.29	+0.30
N(8)	−1.32	−1.25	H(8*A*)	+0.52	+0.51
N(9)	−1.37	−1.37	H(8*B*)	+0.53	+0.51
N(15)	−1.36	−1.28	H(9*A*)	+0.51	+0.51
N(16)	−1.03	−1.14	H(9*B*)	+0.52	+0.53
N(18)	−1.37	−1.21	H(15*A*)	+0.53	+0.50
C(2)	+0.73	+0.59	H(15*B*)	+0.51	+0.51
C(4)	+0.32	+0.34	H(18*A*)	+0.53	+0.51
C(5)	−0.40	−0.25	H(18*B*)	+0.53	+0.49
C(7)	+1.36	+1.24			
C(10)	−0.23	−0.25			
C(12)	−0.20	−0.29			
C(13)	−0.11	−0.21			
C(14)	+0.86	+0.76			

† The sum of atomic charges are −0.006 and −0.004 a.u. for famotidine A and B, respectively.

It should also be noted that the ellipticities, $\varepsilon = (\lambda_1/\lambda_2) - 1$, which can be taken to represent the degree of aromaticity in a particular chemical bond, exhibit some differences. Therefore, an alternative explanation of the different geometries of the guanidine amines could be due to different resonance structures in the famotidine polymorphs. However, despite the fact that the ellipticities potentially carry a wealth of valuable information, they are particularly sensitive parameters and are rarely given much emphasis in experimental charge-density studies.

Aside from the few outliers mentioned above, the topological parameters for the intramolecular bonds compare extraordinarily well for the two polymorphs of famotidine, and together represent a coherent picture of the intramolecular bonding in famotidine that will be used in the following. Firstly, it is definitely expected from its large range of bond distances (see Table 2) that sulfur is involved in a variety of different bonding interactions. According to their geometry, the sulfur interactions should be ranked in order of increasing strength as follows: thioether S(11), thiazole S(1), and sulfamoyl S(17)—N and S(17)—O. The topology (both $\rho_{\rm b.c.p.}$ and $\nabla^2\rho_{\rm b.c.p.}$) fully confirms this sequence, except for $\nabla^2\rho_{\rm b.c.p.}$ in the S—O interactions, which are found to be positive, despite displaying the highest $\rho_{\rm b.c.p.}$ values of all S—*X* interactions. As mentioned above, the positive Laplacian at the b.c.p. should indicate a closed-shell interaction, which again is expected to be a weaker interaction than a covalent or open-shell interaction. However, looking again at Fig. 2, it is apparent that the S—O interactions are all shared interactions. The origin of the positive $\nabla^2\rho_{\rm b.c.p.}$ is instead the location of the b.c.p. close enough to the S atom to actually lie in the positive Laplacian region. It is interesting to note that topological analysis of theoretical densities shows the same tendency (Hibbs *et al.*, 2003).

3.2.3. Atomic charges. Table 4 lists the results of the integration of the atomic basins, performed with *TOPXD* (Volkov *et al.*, 2000). There are some differences between the two polymorphs, particularly in the thiazole ring; however, the fragment charges for the thiazole ring (+0.23) as well as the guanidine group (−0.29) are conserved, suggesting that the differences in charges reflect small variations in the pattern of electronic delocalization within these fragments.

It is especially interesting to note the variation in the S atomic charges, which to some extent mirror the different oxidation states of sulfur. This is contrasted by the simple monopole charges, occasionally used to obtain a crude estimate of atomic charge using the following relation: $q(P_v) = N - P_v$, where P_v is the refined monopole parameter and N is the number of valence electrons in the neutral atom, which in this case does not offer any significant distinction between the different sulfur atomic types [thiazole S(1): +0.21, +0.34; thioether S(11): +0.11, +0.17; sulfamoyl S(17): +0.29, +0.72, listed for A, B, respectively].

A comparison of the Bader charges, obtained by integration over the topological atomic basin volumes with the pseudoatom monopole charges, is also relevant for the other atoms in the structure. Table 4 shows that C(2) has a significant build up of topological positive charge and is the most positive atom in the thiazole ring, while the pseudoatom monopole charges exhibit quite the opposite trend, which indicates that C(2) has a negative charge comparable to those of both C(5) and N(3). This is unexpected, as all three neighbours of C(2) based on their individual electronegativity will draw electrons from C(2). The Bader topological charges unambiguously arrange the H atoms in two fractions, separating the sp^3 C-bonded H atoms [$q(\Omega) = +0.2$] from the H atoms bonded to N [$q(\Omega) = +0.5$], while H(5) is in between. Again, such a distinction is not possible using the monopole charges.

In the literature, atomic charges calculated using a QM/MM method (QM charges not shown) are given (Ferenczy *et al.*, 2000), and a comparison with the experimental Bader charges is interesting. The QM charges exhibit a trend similar to the monopole charges being of similar sign but smaller in magnitude compared to the Bader charges. However, the QM charges compare extremely well with the Bader charges for both O atoms and for S(17). On the other hand, QM finds N(16) to be the most negative N atom, exactly contrary to the current experiment.

3.2.4. Electrostatic potential. The present work has been performed partly with the intention to analyse the possible interaction of famotidine with the histamine H_2 receptor. For this purpose, the topological analysis described above is not sufficient and additional information is needed. One method that has proved promising in recent years is the analysis of the electrostatic potential on the molecular surface, a procedure that has been pioneered by the group of Politzer & Murray (2002) on theoretical data, while applications of this method to experimental data are scarce (Spasojevic de Bire *et al.*, 2002; Hibbs *et al.*, 2004). The idea behind this method is that drug–receptor interactions are non-covalent in nature and that the drug molecule has to fit in both a geometric and an electrostatic sense to the receptor in a key–lock mode.

Fig. 3 shows the experimentally derived molecular electrostatic potential for both A and B mapped onto the isodensity surfaces of 0.00675 e Å^{-3}. This particular value is the one value most commonly occurring in the literature and the one that Bader proposed in his original work on molecular surfaces (Bader *et al.*, 1987). Both polymorphs exhibit a large charge separation with a large pronounced electronegative area separated from a similar-sized mainly electropositive surface, explaining the large molecular dipole moment in the crystalline setting. Famotidine A (Fig. 3*a*) is the more elongated molecule and the molecular surface shape is significantly different from that of famotidine B (Fig. 3*b*), which resembles a square. Furthermore, the electronegative (blue) regions of famotidine A are considerably less negative (average −40 kJ mol^{-1}) compared to famotidine B (average −55 kJ mol^{-1}), found by a statistical evaluation of both surfaces. It is thus evident that the two conformations of famotidine are so very different – both geometrically and electrostatically – that they cannot dock with a receptor molecule in any similar way. In addition, there are a wealth of maxima and minima in the electrostatic potential on both surfaces that can be localized and implemented in a subsequent correlation study. However, such an analysis requires the study of a sequence of similarly functioning drugs, which is currently being carried out and will be published separately.

3.2.5. Intermolecular interaction energy and crystal dipole moment. One highly important property of a molecule in relation to drug action is the molecular dipole moment, which influences the solubility of a particular molecule in a certain solvent (blood, fat *etc*.). It is a property that can be easily calculated for a single molecule but it is a much harder task to extrapolate to its value *in vitro*. It is known that the dipole moment is enhanced upon crystal formation (Gatti *et al.*, 2001) and it can be speculated that the dipole moment in solution is similar to the dipole moment in a crystal. Thus, we have calculated the dipole moments for both polymorphs resulting in values of 18.1 (7) and 20.8 (15) D for famotidine A and B, respectively. This represents a significant magnification compared to the single-molecule dipole moments, which have been calculated as 7.3 and 7.9 D for A and B, respectively, using fixed experimental geometries. Geometry optimizations reduce these values to 4.2 and 4.9 D, respectively. Thus, the crystalline environment influences the molecular dipole moment similarly in both polymorphs and any distinction of the two species does not seem feasible based on the dipole moment alone.

Using the experimental charge-density approach, the intermolecular interaction energy ($E_{\rm int}$) can be calculated from the multipole description of the molecular charge densities (Abramov *et al.*, 2000). This reveals that famotidine A is by far (−174.3 *versus* −83.0 kJ mol^{-1}) the more stable crystal configuration, essentially due to an enhanced electrostatic contribution. This relates well to a study of the morphological stability of famotidine, which showed that

famotidine A is the thermodynamically preferred form (Hegedűs *et al.*, 1989).

4. Conclusions

This study outlines a comparison of the independently derived experimental electron densities for the two known conformational polymorphs of the commercial anti-ulcer drug famotidine. Despite the large differences in molecular conformation, the analysis revealed excellent consistency in intramolecular electronic structure and bonding properties, such as topological parameters and integrated atomic charges, for the two polymorphs. It is thus indicated that a low-temperature high-resolution accurate single-crystal X-ray diffraction experiment using a conventional source can indeed provide the high-quality data needed for an electron-density refinement, free of systematic errors that may potentially hamper a positive result.

The topological analysis of famotidine A and B finds essentially no differences in intramolecular bonding due to the differences in molecular conformation. Similarly, the atomic charges deviate only very slightly between polymorphs, again showing that the conformational transformation of the molecule has no influence on the atomic properties. Even the molecular dipole moment reveals no dependency on conformation.

The molecular electrostatic potential mapped on top of the molecular surface is introduced as a method of both qualitative and quantitative analysis. In contrast to the topological analysis of the molecule, this method clearly reveals the electrostatic consequences of the conformational polymorphism of famotidine, and shows that only one of the conformations can be regarded as the docking conformation at the receptor. This method may provide a tool that is a potentially important source of information on the mechanism of drug–receptor interaction and work is under way to elucidate this further.

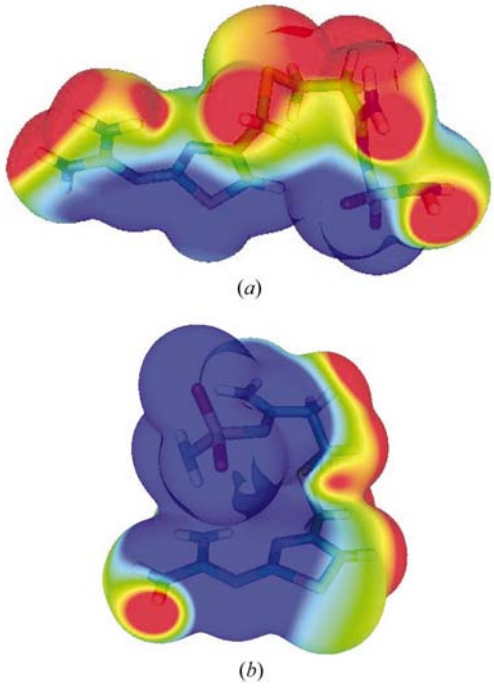

Figure 3
Molecular electrostatic potential mapped on the isodensity surface of 0.00675 e Å^{-3} for famotidine A (*a*) and B (*b*). The colour scheme ranges from blue (negative) *via* green (neutral) to red (positive) with values in the ranges: $-99 \rightarrow +173$ kJ mol^{-1} for A and $-117 \rightarrow +179$ kJ mol^{-1} for B.

The authors are grateful to Dr Bela Hegedűs for the kind donation of the crystals. The Australian Research Council is thanked for funding this work and the Australian Centre for Advanced Computing and Communications for generous allocation of computing time. JO also thanks the Danish Research Council for funding.

References

Abramov, Y. A., Volkov, A., Wu, G. & Coppens, P. (2000). *Acta Cryst.* A**56**, 585–591.
Allen, F. H., Kennard, O., Watson, D. G., Brammer, L., Orpen, A. G. & Taylor, R. (1987). *J. Chem. Soc. Perkin Trans. 2*, pp. S1–S9.
Bader, R. F. W. (1990). *Atoms in Molecules. A Quantum Theory*. New York: Oxford University Press.
Bader, R. F. W., Caroll, M. T., Cheeseman, J. R. & Chang, C. (1987). *J. Am. Chem. Soc.* **109**, 7968.
Blessing, R. H. (1997). *J. Appl. Cryst.* **30**, 421–426.
Brimblecombe, R. W., Duncan, W. A., Durant, G. J., Ganellin, C. R., Parsons, M. E. & Black, J. W. (1975). *Br. J. Pharmacol.* **53**, 435–436.
Bruker (1998). *SAINT*. Bruker AXS Inc., Madison, Wisconsin, USA.
Clementi, E. & Roetti, C. (1974). *At. Data Nucl. Data Tables*, **14**, 177–478.
El Haouzi, A., Hansen, N. K., Le Henaff, C. & Protas, J. (1996). *Acta Cryst.* A**52**, 291–301.
Espinosa, E., Molins, E. & Lecomte, C. (1997). *Phys. Rev. B*, **56**, 1820–1833.
Ferenczy, G. G., Párkányi, L., Ángyán, J. G., Kálmán, A. & Hegedűs, B. (2000). *J. Mol. Struct. (Theochem)*, **503**, 73–79.
Figgis, B. N., Iversen, B. B., Larsen, F. K. & Reynolds, P. A. (1993). *Acta Cryst.* B**49**, 794–806.
Gatti, C., Destro, R. & May, E. (2001). *J. Am. Chem. Soc.* **123**, 12248–12254.
Gedeon Richter Ltd (1986). European Patent 0 256 747.
Gopalan, R. S., Kulkarni, G. U. & Rao, C. N. R. (2000). *ChemPhysChem*, **1**, 127–135.
Hambley, T. W., Hibbs, D. E., Turner, P., Howard, S. T. & Hursthouse, M. B. (2002). *J. Chem. Soc. Perkin Trans. 2*, pp. 235–239.
Hansen, N. K. & Coppens, P. (1978). *Acta Cryst.* A**34**, 909–921.
Hegedűs, B., Bod, P., Harsányi, K., Peter, I., Kálmán, A. & Párkányi, L. (1989). *J. Pharm. Biomed. Anal.* **7**, 563.
Hibbs, D. E., Austin-Woods, C. J., Platts, J. A., Overgaard, J. & Turner, P. (2003). *Chem. Eur. J.* **9**, 1075–1084.
Hibbs, D. E., Overgaard, J., Platts, J. A., Waller, M. P. & Hursthouse, M. B. (2004). *J. Phys. Chem. B*, **108**, 3663–3672.
Hirshfeld, F. L. (1976). *Acta Cryst.* A**32**, 239–244.
Koritsanszky, T., Howard, S. T., Macchi, P., Gatti, C., Farrugia, L. J., Mallinson, P. R., Volkov, A., Su, Z., Richter, T. & Hansen, N. K. (2003). *XD. A Computer Program Package for Multipole Refinement and Analysis of Charge Densities from X-ray Diffraction Data*, Free University of Berlin, Germany.
Kulkarni, G. U., Gopalan, R. S. & Rao, C. N. R. (2000). *J. Mol. Struct. (Theochem)*, **500**, 339–362.
Kulkarni, G. U., Kumaradhas, P. & Rao, C. N. R. (1998). *Chem. Mater.* **10**, 3498–3505.

Leusser, D., Henn, J., Kocher, N., Engels, B. & Stalke, D. (2004). *J. Am. Chem. Soc.* **126**, 1781–1793.
Leusser, D., Walfort, B. & Stalke, D. (2002). *Angew. Chem. Int. Ed. Engl.* **42**, 2079–2082.
Macchi, P., Proserpio, D. M. & Sironi, A. (1998). *J. Am. Chem. Soc.* **120**, 13429–13435.
McCormack, K. L., Mallinson, P. R., Webster, B. C. & Yufit, D. S. (1996). *J. Chem. Soc. Faraday Trans.* **96**, 1709–1716.
Pillet, S., Souhassou, M., Pontillon, Y., Caneschi, A., Gatteschi, D. & Lecomte, C. (2001). *New J. Chem.* **25**, 131–143.
Politzer, P. & Murray, J. S. (2002). *Theo. Chem. Acc.* **108**, 134.
Scherer, W., Spiegler, M., Pedersen, B., Tafipolsky, M., Hieringer, W., Reinhard, B., Downs, A. J. & McGrady, G. S. (2000). *Chem. Commun.* pp. 635–636.
Sheldrick, G. M. (1997). *SHELX97, Programs for Crystal Structure Analysis* (Release 97-2). University of Göttingen, Germany.
Spasojevic de Bire, A., Bouhmaida, N., Kremenovic, A., Morgant, G. & Ghermani, N. E. (2002). *J. Phys. Chem. A*, **106**, 12170.
Volkov, A., Gatti, C., Abramov, Yu. A. & Coppens, P. (2000). *Acta Cryst.* A**56**, 252.
Whitten, A. E., Dittrich, B., Spackman, M. A., Turner, P. & Brown, T. C. (2004). *Dalton Trans.* pp. 23–29.